Supplementary Information

Suppressing bias stress degradation in high performance solution processed organic transistors operating in air

Hamna F. Iqbal[1], Qianxiang Ai[2], Karl J. Thorley[2], Hu Chen[3], Iain McCulloch[3,4], Chad Risko[2], John E. Anthony[2] and Oana D. Jurchescu[1,*]

[1]Department of Physics and Center for Functional Materials, Wake Forest University, Winston Salem, NC 27109, USA

[2]Department of Chemistry and Center for Applied Energy Research (CAER), University of Kentucky, Lexington, KY 40506, USA

[3]King Abdullah University of Science and Technology, KAUST Solar Center (KSC), Thuwal 23955-6900, Saudi Arabia

[4]Department of Chemistry, Chemistry Research Laboratory, University of Oxford, Oxford, OX1 3TA, UK

*Corresponding author email: Jurchescu@wfu.edu

Contents:

Supplementary Discussion 1: Operational stability tests on unencapsulated TnHS BDT trimer devices in ambient air

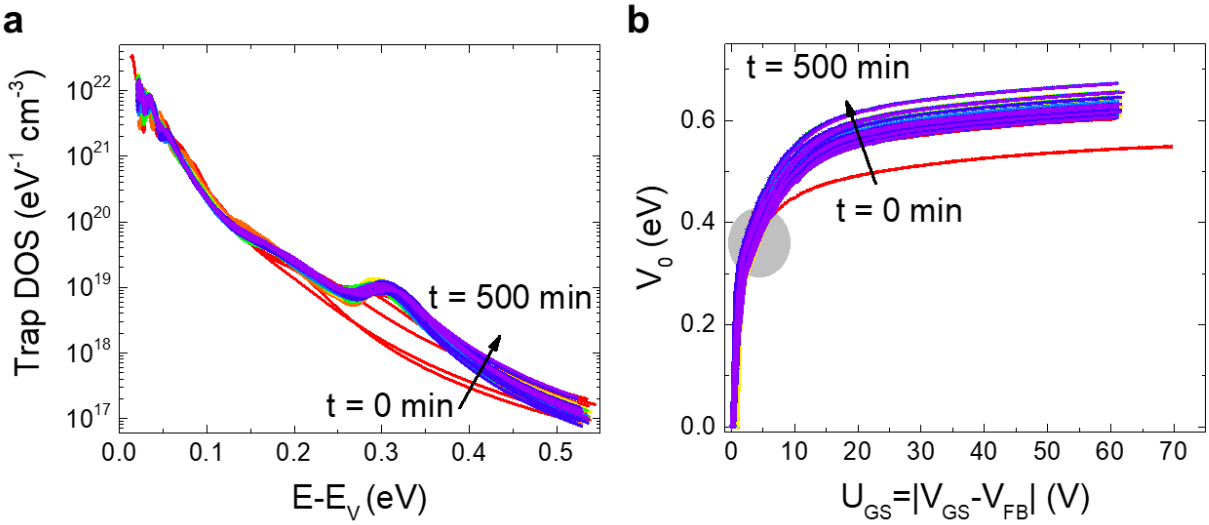

Supplementary Figure 1 | Trap DOS analysis performed on an unencapsulated TnHS BDT trimer device operating in ambient air for 500 min. a, DOS spectra evaluated during repeated transistor operation. **b,** The gate-voltage dependent interface potential function. The gray shaded area highlights a subtle change in the curvature of the plots giving rise to the peak in the corresponding DOS spectrum.

Supplementary Table 1. Model parameters used for the double exponential and Gaussian distributions employed to model the DOS spectra of a device operated in ambient air. The spectrum at t = 500 min was modelled using only a double exponential distribution and therefore the Gaussian parameters are not applicable.

Model Parameter	t = 0 min	t = 500 min
N_1 (eV^{-1} cm^{-3})	2.0×10^{22}	4.8×10^{22}
E_1 (meV)	25.0	17.5
N_2 (eV^{-1} cm^{-3})	5.2×10^{19}	5.0×10^{20}
E_2 (meV)	85.5	64.9
A (eV^{-1} cm^{-3})	N/A	7.0×10^{18}
E_{peak} (eV)	N/A	0.31
σ (meV)	N/A	25.0

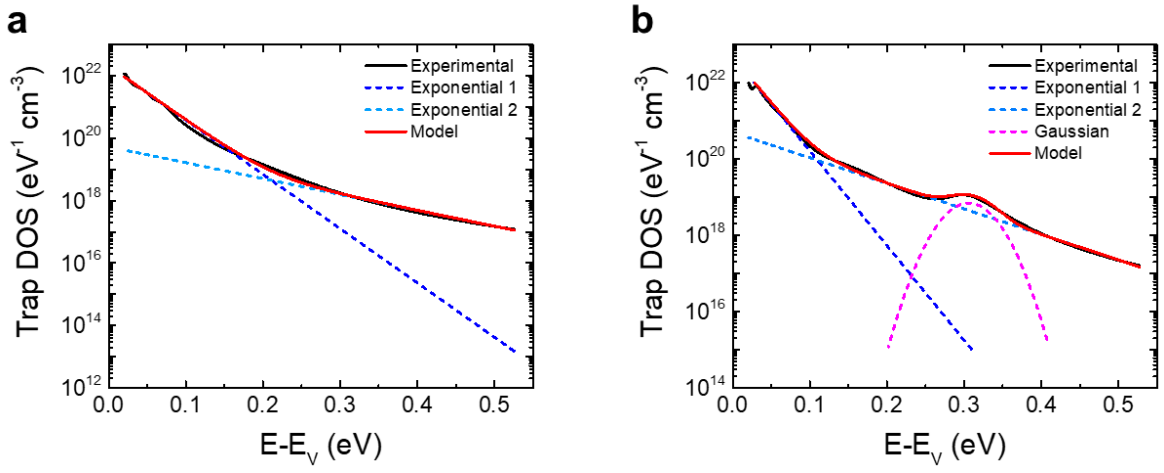

Supplementary Figure 2 | Modeling of the trap DOS spectra of an unencapsulated TnHS BDT trimer device operating in ambient air. Model fit (red solid lines) to experimental DOS spectrum (solid black lines) of a device at different times during operation: **a**, t = 0 min and **b**, after t = 500 min of operation. Broken lines represent the individual distribution functions employed for the modelling.

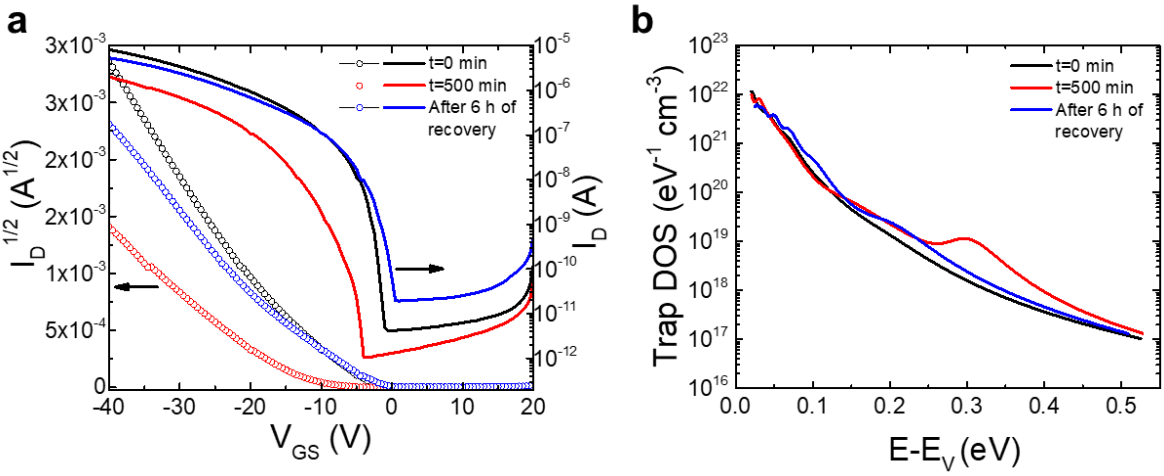

Supplementary Figure 3 | Transistor characteristics of an unencapsulated TnHS BDT trimer device during repeated measurements and after recovery. a, Saturation regime transfer characteristics (V_{DS} =-60 V) of a device at t = 0 min (black), t = 500 min (red) of operation, and after 6 h of device recovery (blue). The left and right axes show the square root and the logarithm of I_D respectively. **b**, Trap DOS spectra evaluated at t = 0 min (black), t = 500 min (red) of operation, and after 6 h of device recovery (blue).

Supplementary Discussion 2: Operational stability tests on unencapsulated TnHS BDT trimer devices in vacuum

Supplementary Table 2. Model parameters used for the double exponential distributions employed to model the DOS spectra of a device operated in vacuum.

Model Parameter	t = 0 min	t = 500 min
N_1 (eV^{-1} cm^{-3})	1.5×10^{22}	7.4×10^{20}
E_1 (meV)	20.0	9.1
N_2 (eV^{-1} cm^{-3})	3.9×10^{20}	1.8×10^{20}
E_2 (meV)	53.4	47.5

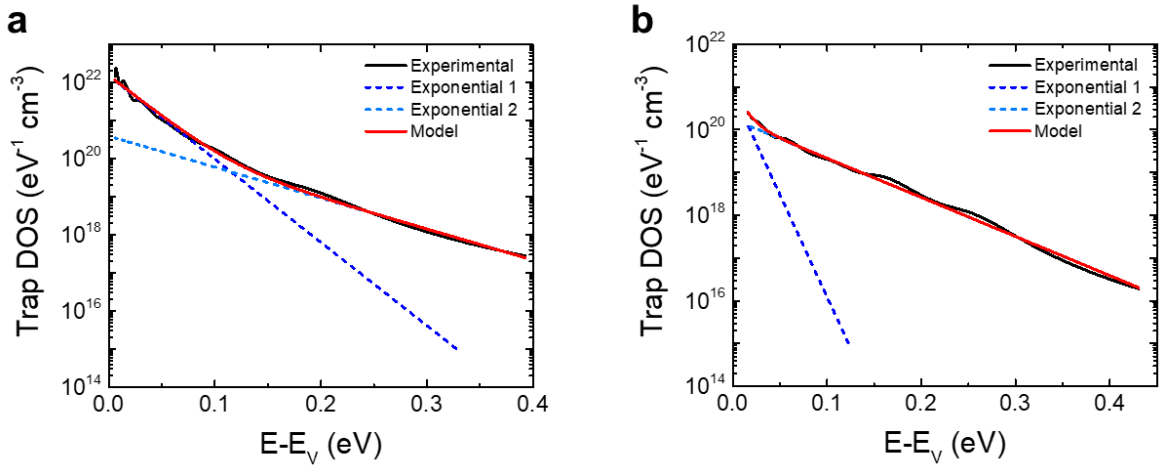

Supplementary Figure 4 | Modeling of the trap DOS spectra of an unencapsulated device operating in vacuum. Model fit (red solid lines) to experimental DOS spectrum (solid black lines) of a device at different times during operation: **a**, t = 0 min and **b**, after t = 500 min of operation. Broken lines represent the individual distribution functions employed for the modelling.

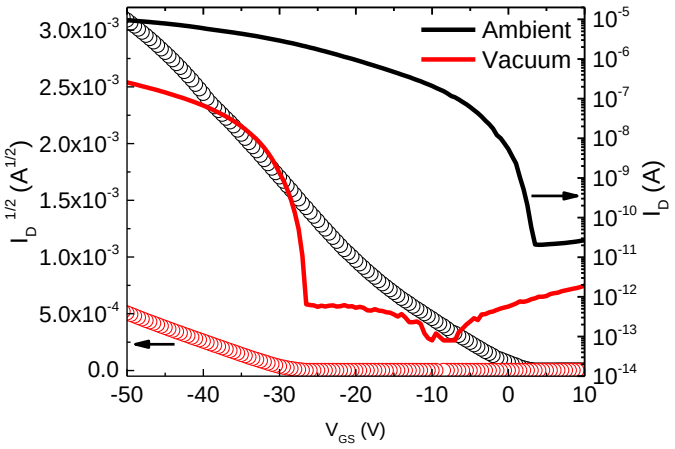

Supplementary Figure 5 | Comparison of the current-voltage characteristics of an unencapsulated device measured under different environments. Saturation regime transfer characteristics (I_D vs V_{GS} at V_{DS}=-60 V) under ambient air (black) and vacuum (red). The left and right axes show the square root and the logarithm of I_D respectively.

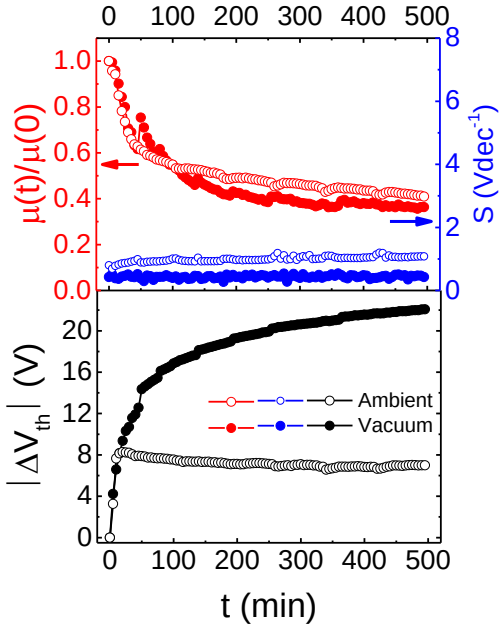

Supplementary Figure 6 | Time evolution of device metrics of an unencapsulated TnHS BDT trimer device during repetitive transistor operation under different environments. Open circles and solid circles represent measurements obtained in ambient air and vacuum, respectively. Time evolution of the mobility μ normalized to the value at t = 0 min (red), subthreshold slope S (blue) and magnitude of threshold voltage shifts $|\Delta V_{th}|$ (black) are shown.

Supplementary Discussion 3: Environmental stability tests on unencapsulated TnHS BDT trimer devices

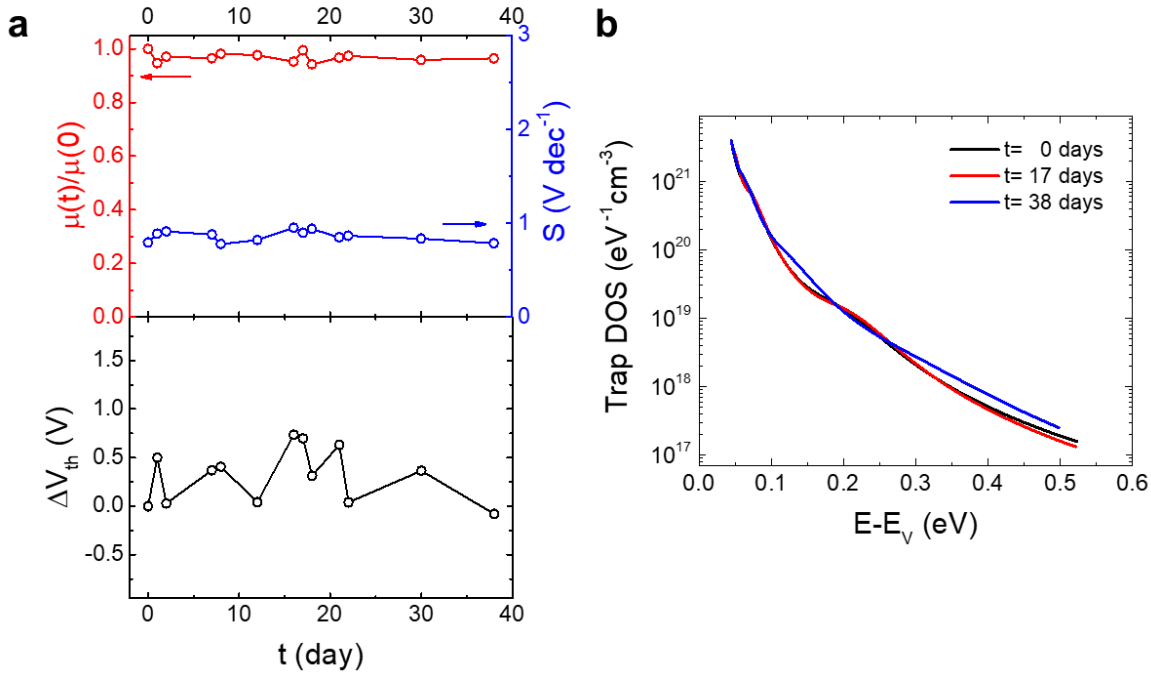

Supplementary Figure 7 | Time evolution of device metrics and trap DOS spectrum of an unencapsulated TnHS BDT trimer device during environmental stability tests. a, Time evolution of the mobility μ normalized to the value at t = 0 min (red), subthreshold slope *S* (blue) and threshold voltage shifts ΔV_{th} (black) are shown. **b**, Trap DOS spectra evaluated over the course of environmental stability tests performed for 38 days.

Supplementary Discussion 4: Computational details

Density functional theory (DFT) calculations were carried out on isolated molecules and bulk crystal structures. Molecular calculations were performed at the ωB97XD/Def2SVP level of theory as implemented in Gaussian 16[3–5]. Bulk crystal calculations were carried out with Vienna *Ab-initio* Simulation Package[6–9], making use of the Perdew, Burke, and Ernzerhof exchange-correlation functional[10]. The electron-ion interactions were described with the projector augmented wave method[11]. The kinetic energy cutoff for the plane-wave basis set was set to 520 eV, and a Gaussian smearing with a width of 50 meV was employed. The D3 correction was employed with BJ-damping to describe the dispersion forces[12]. The convergence criterion of the total energy was set to 10^{-5} eV in the self-consistent field loop, and that of forces during relaxation was set to 0.01 eV/Å. Considering the large volume of the TnHS BDT trimer unit cell, Gamma centered 2 × 2 × 1 mesh was used to sample the Brillouin zone. Unit cells are also used for charged defects as the shortest translation vector is larger than 10 Å.

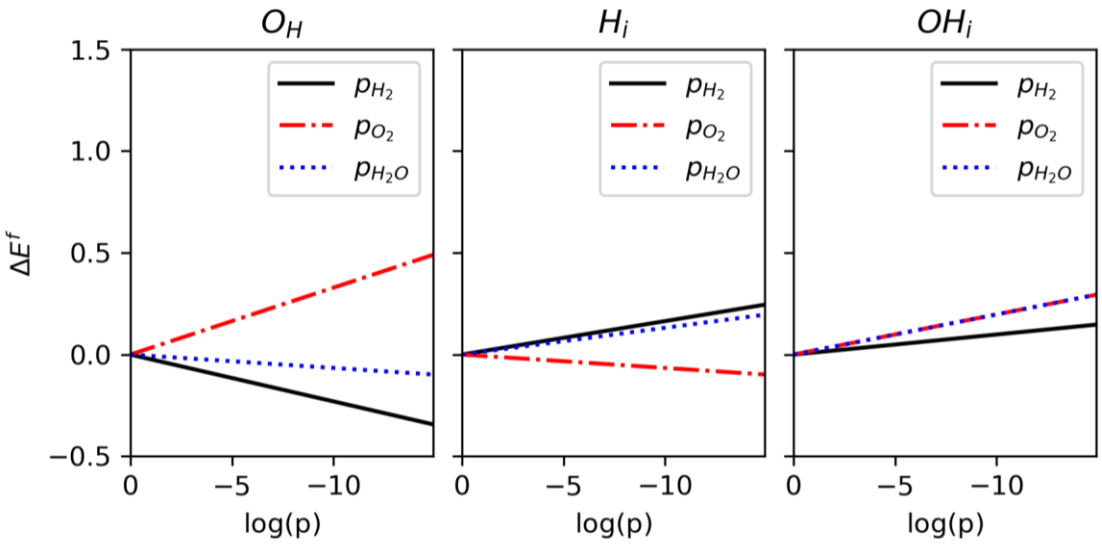

Supplementary Figure 8 | Linear relationships between ΔE^f and log (P) for the three potential chemical defects of TnHS BDT trimer.

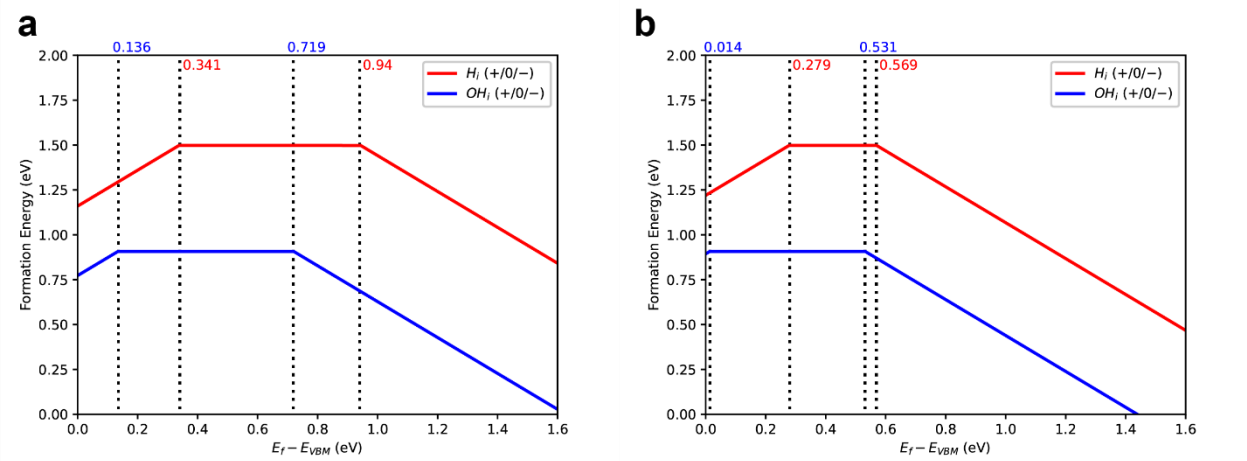

Supplementary Figure 9 | Defect formation energies as a function of Fermi level relative to the valence band edge for H_i and OH_i defects in TnHS BDT trimer at $P_{O_2} = P_{H_2} = P_{H_2O} = 10^{-10}$ Pa. a, Defect formation energies without correction and **b**, after applying the correction scheme (FNV) proposed by Freysoldt *et al.*[13,14], as implemented in PyCDT[15]. Transition levels are labeled with vertical dotted lines. Only monocation or monoanion states are considered.

Supplementary Discussion 5: Operational stability tests on unencapsulated vs. encapsulated TnHS BDT trimer device in air

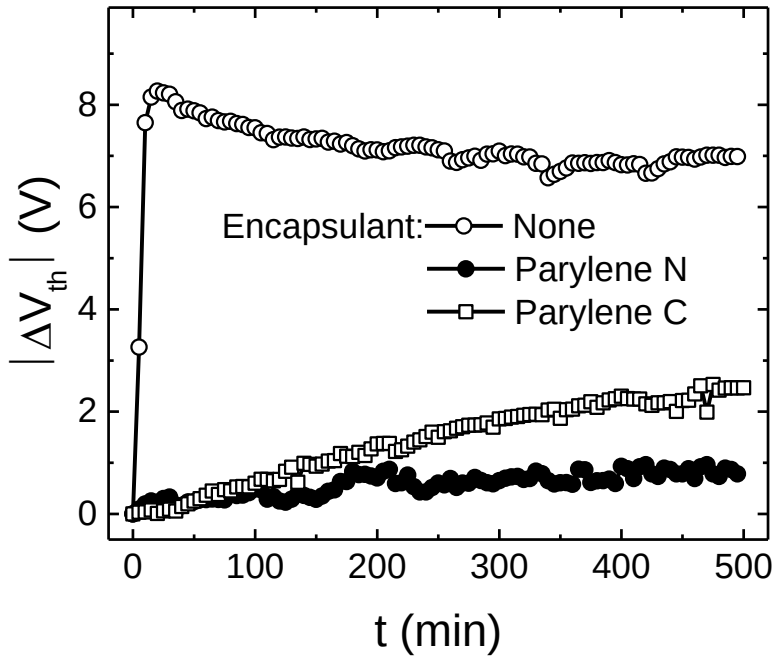

Supplementary Figure 10 | Comparison of threshold voltage shifts of unencapsulated and encapsulated TnHS BDT trimer devices during repetitive transistor operation for 500 min in air. An unencapsulated device (open circles) yielded a shift of ΔV_{th} = - 8 V while devices encapsulated with parylene N (solid circles) and parylene C (open squares) yielded shifts of ΔV_{th} = - 0.9 V and ΔV_{th} = - 2.5 V respectively.

Supplementary Discussion 6: Hysteresis in current-voltage characteristics of TnHS BDT trimer devices

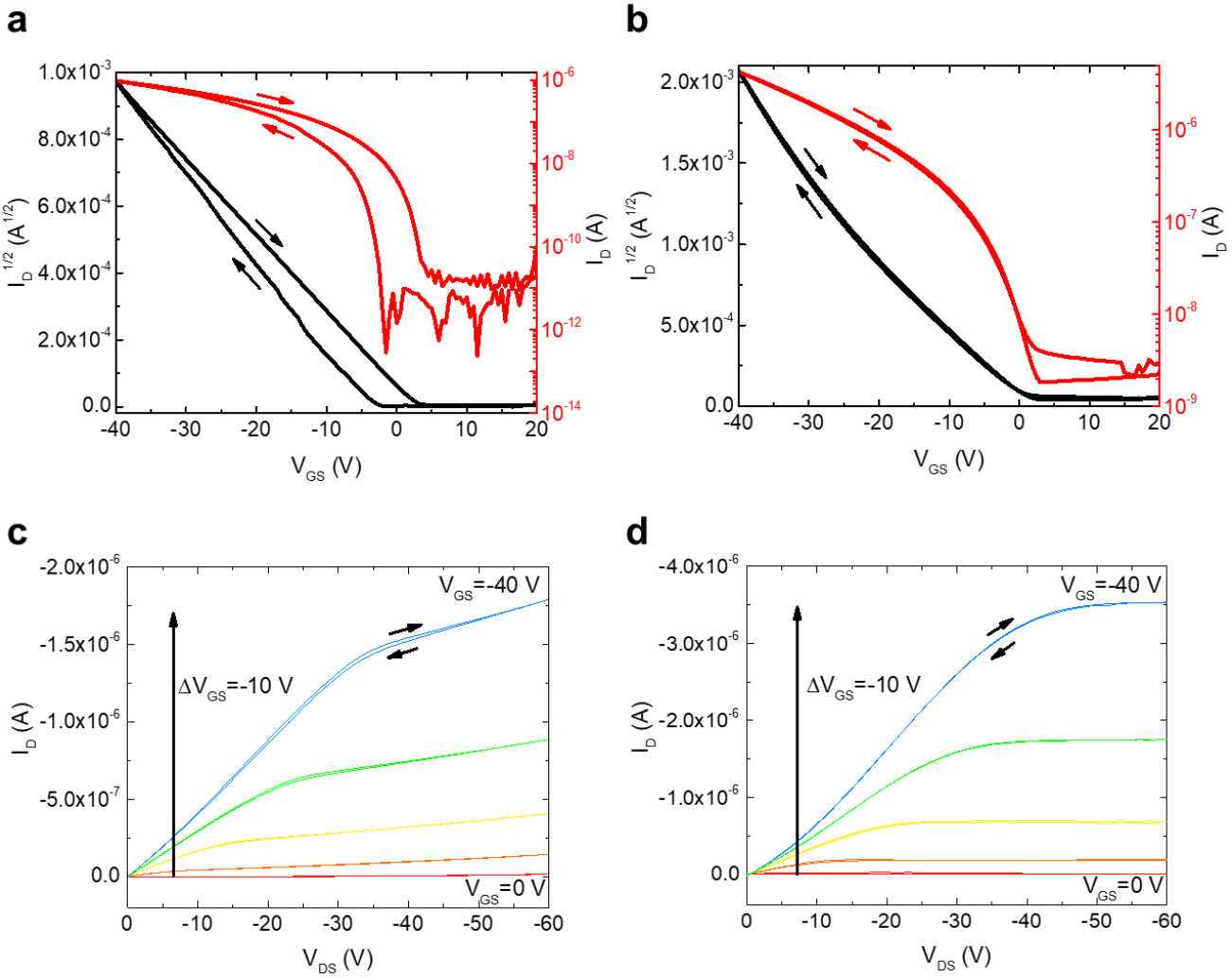

Supplementary Figure 11 | Hysteresis in current-voltage characteristics of unencapsulated and parylene N-encapsulated TnHS BDT trimer devices. **a**, Hysteresis in the transfer characteristics of an unencapsulated device in comparison to **b**, a device encapsulated with parylene N. **c**, Hysteresis in the transport characteristics of the unencapsulated device in comparison to **d**, the encapsulated device.

Supplementary Discussion 7: Bias stress measurements on TnHS BDT trimer devices

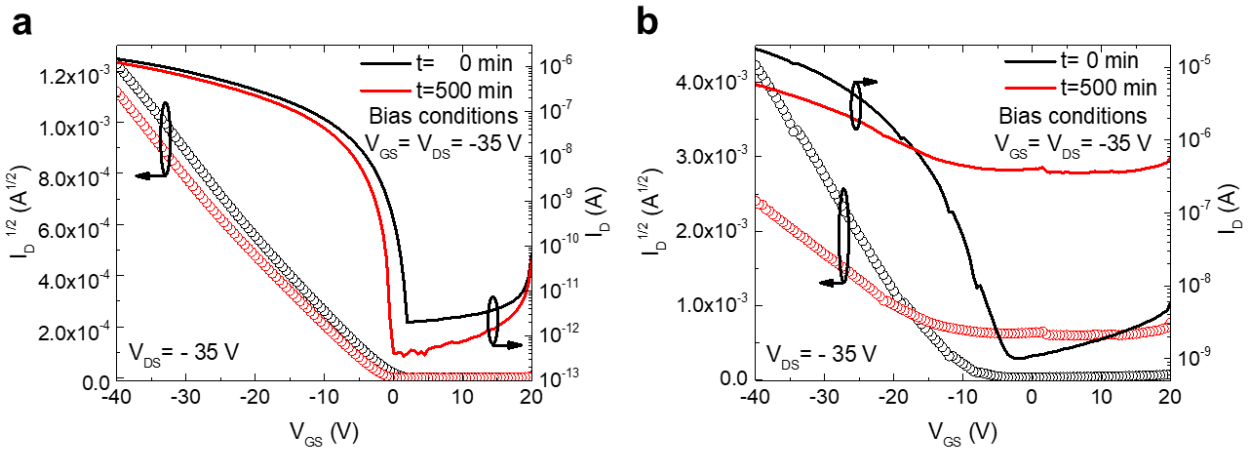

Supplementary Figure 12 | Bias stress measurements on a TnHS BDT trimer device encapsulated with parylene C compared to an unencapsulated device. a, Transfer characteristics of a device encapsulated with parylene C acquired at V_{DS} = -35 V prior to stressing (black) and after 500 min of stressing (red) under the application of a continuous drain voltage and a dynamic gate bias pulsed at 10 s interval at V_{DS} = V_{GS} = - 35 V. The threshold voltage shift is ΔV_{th} = - 1.3 V**. b,** Transfer characteristics of an unencapsulated device acquired at V_{DS} = - 35 V prior to stressing (black) and after 500 min of stressing (red) under identical bias conditions. The threshold voltage shift is ΔV_{th} = + 4.9 V**.**

Supplementary Discussion 8: Bilayer dielectric IDT-BT devices

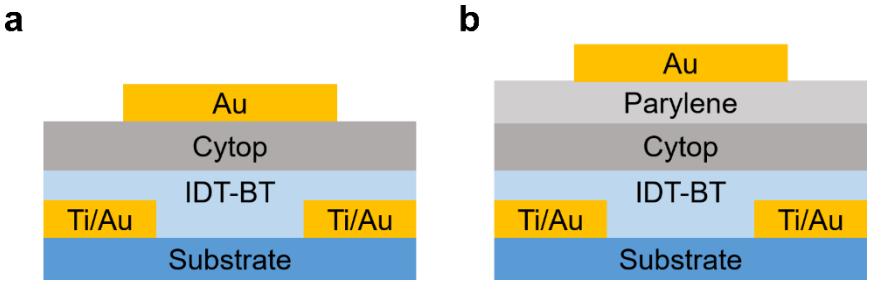

Supplementary Figure 13 | IDT-BT device geometries fabricated and tested. a, Bottom-contact, top-gate device with Cytop dielectric. **b,** Bottom-contact, top-gate device with bilayer dielectric consisting of Cytop and parylene.

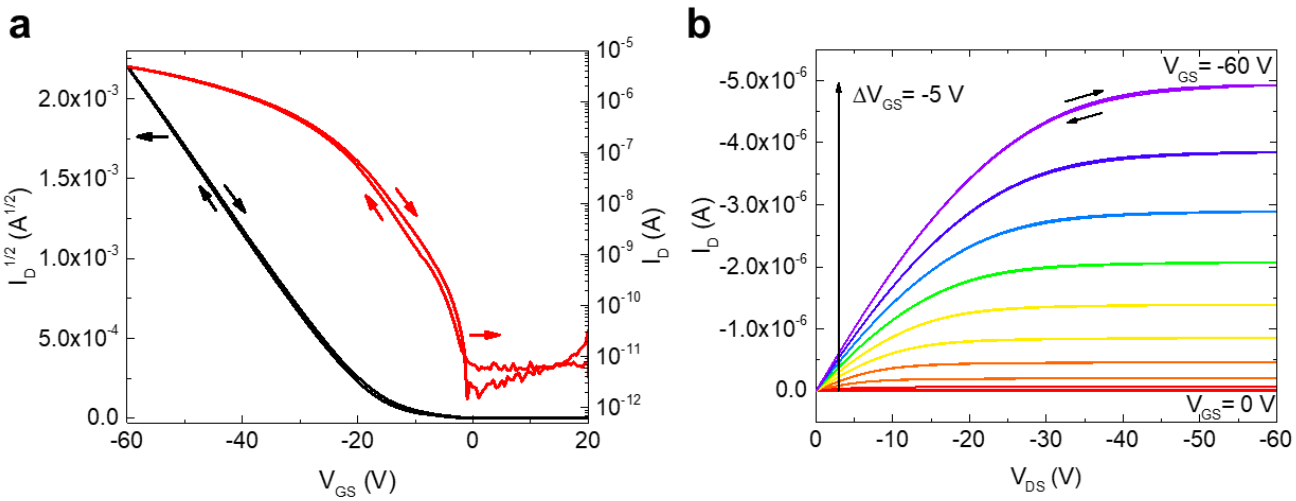

Supplementary Figure 14 | Hysteresis in current-voltage characteristics of a bilayer dielectric IDT-BT device. **a**, Hysteresis in the transfer characteristics. **b**, Hysteresis in the output characteristics.

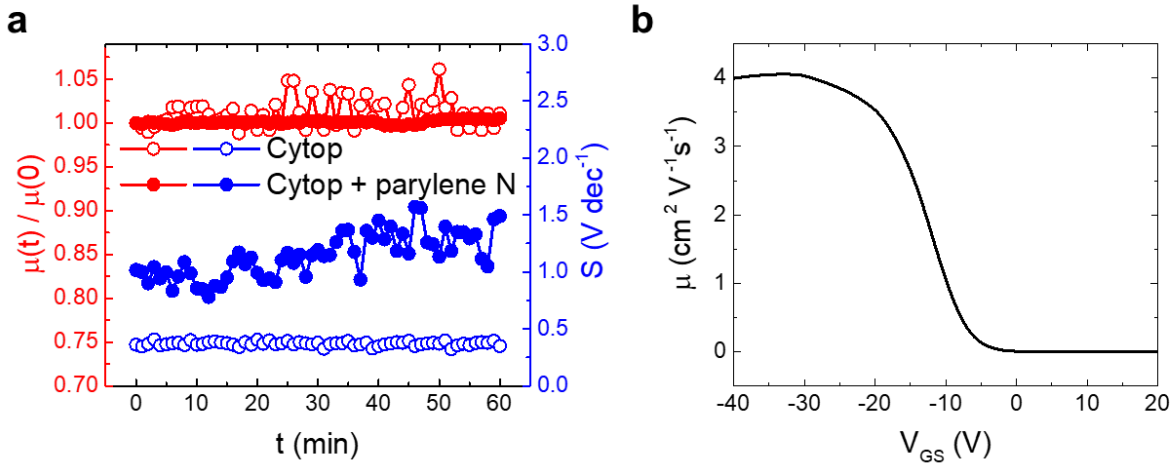

Supplementary Figure 15 | Time evolution of device metrics and the dependency of mobility on gate-voltage in IDT-BT devices fabricated with different dielectrics. a, Left and right axes show the change in normalized mobility and subthreshold slope respectively of a Cytop-only device (open circles) in comparison to a bilayer dielectric device (solid circles). **b**, Gate voltage dependence of the mobility of the bilayer dielectric device with L = 100 μm, W = 200 μm and an equivalent areal capacitance of C_i=1.26 nF cm^{-2}.

Supplementary References

1. Massey, L. K. *Permeability Properties of Plastics and Elastomers, 2nd Ed.: A Guide to Packaging and Barrier Materials*. (Elsevier Science, 2003).
2. McKeen, L. W. *Permeability Properties of Plastics and Elastomers: Fourth Edition*. *Permeability Properties of Plastics and Elastomers: Fourth Edition* (Elsevier Science, 2016).
3. Chai, J.-D. & Head-Gordon, M. Long-range corrected hybrid density functionals with damped atom–atom dispersion corrections. *Phys. Chem. Chem. Phys.* **10**, 6615 (2008).
4. Dunning, T. H. Gaussian basis sets for use in correlated molecular calculations. I. The atoms boron through neon and hydrogen. *J. Chem. Phys.* **90**, 1007–1023 (1989).
5. Frisch, M. J. *et al.* G16_C01. Gaussian 16, Revision C.01, Gaussian, Inc., Wallin (2016).
6. Kresse, G. & Hafner, J. Ab initio molecular dynamics for liquid metals. *Phys. Rev. B* **47**, 558–561 (1993).
7. Kresse, G. & Joubert, D. From ultrasoft pseudopotentials to the projector augmented-wave method. *Phys. Rev. B* **59**, 1758–1775 (1999).
8. Kresse, G. & Furthmüller, J. Efficient iterative schemes for ab initio total-energy calculations using a plane-wave basis set. *Phys. Rev. B* **54**, 11169–11186 (1996).
9. Kresse, G. & Furthmüller, J. Efficiency of ab-initio total energy calculations for metals and semiconductors using a plane-wave basis set. *Comput. Mater. Sci.* **6**, 15–50 (1996).
10. Perdew, J. P. *et al.* Erratum: Atoms, molecules, solids, and surfaces: Applications of the generalized gradient approximation for exchange and correlation. *Phys. Rev. B* **48**, 4978–4978 (1993).
11. Blöchl, P. E. Projector augmented-wave method. *Phys. Rev. B* **50**, 17953–17979 (1994).
12. Grimme, S., Ehrlich, S. & Goerigk, L. Effect of the damping function in dispersion corrected density functional theory. *J. Comput. Chem.* **32**, 1456–1465 (2011).
13. Freysoldt, C., Neugebauer, J. & Van de Walle, C. G. Fully Ab Initio Finite-Size Corrections for

Charged-Defect Supercell Calculations. *Phys. Rev. Lett.* **102**, 016402 (2009).

14. Freysoldt, C., Neugebauer, J. & Van de Walle, C. G. Electrostatic interactions between charged defects in supercells. *Phys. status solidi* **248**, 1067–1076 (2011).

15. Broberg, D. *et al.* PyCDT: A Python toolkit for modeling point defects in semiconductors and insulators. *Comput. Phys. Commun.* **226**, 165–179 (2018).